Tsunami Damage Investigation of Built-Up Areas Using Multitemporal Spaceborne Full Polarimetric SAR Images

Si-Wei Chen, *Student Member, IEEE*, and Motoyuki Sato, *Fellow, IEEE*

***Abstract*—This paper explores the use of full polarimetric synthetic aperture radar (PolSAR) images for tsunami damage investigation from the polarimetric viewpoint. The great tsunami induced by the earthquake of March 11th, 2011, which occurred beneath the Pacific off the northeastern coast of Japan, is adopted as the study case using the Advanced Land Observing Satellite/Phased Array type L-band Synthetic Aperture Radar multitemporal PolSAR images. The polarimetric scattering mechanism changes were quantitatively examined with model-based decomposition. It is clear that the observed reduction in the double-bounce scattering was due to a change into odd-bounce scattering, since a number of buildings were completely washed away, leaving relatively a rough surface. Polarization orientation (PO) angles in built-up areas are also investigated. After the tsunami, PO angle distributions from damaged areas spread to a wider range and fluctuated more strongly than those from the before-tsunami period. Two polarimetric indicators are proposed for damage level discrimination at the city block scale. One is the ratio of the dominant double-bounce scattering mechanism observed after-tsunami to that observed before-tsunami, which can directly reflect the amount of destroyed ground-wall structures in built-up areas. The second indicator is the standard deviation of the PO angle differences, which is used to interpret the homogeneity reduction of PO angles. Experimental results from after- and before-tsunami comparisons validate the efficiency of these indexes, since the built-up areas with different damage levels can be well discriminated. In addition, comparisons between before-tsunami pairs further confirm the stability of the two polarimetric indexes over a long temporal duration. These interesting results also demonstrate the importance of full polarimetric information for natural disaster assessment.**

***Index Terms*—Damage assessment, model-based decomposition, natural disaster, polarimetry, polarization orientation angle, synthetic aperture radar (SAR), urban area.**

Manuscript received February 28, 2012; revised May 31, 2012; accepted June 24, 2012. Date of publication November 15, 2012; date of current version March 21, 2013. This work was supported in part by the Japan Society for the Promotion of Science (JSPS) Grant-in-Aid for Scientific Research (A) 23246076.

S.-W. Chen is with the State Key Laboratory of Complex Electromagnetic Environment Effects on Electronics and Information System, College of Electronic Science and Engineering, National University of Defense Technology, Changsha, Hunan 410073, China, and also with the Graduate School of Environmental Studies, Tohoku University, Sendai 980-8576, Japan (e-mail: chenswnudt@163.com).

M. Sato is with the Center for Northeast Asian Studies, Tohoku University, Sendai 980-8576, Japan (e-mail: sato@cneas.tohoku.ac.jp).

Color versions of one or more of the figures in this paper are available online at http://ieeexplore.ieee.org.

Digital Object Identifier 10.1109/TGRS.2012.2210050

I. Introduction

THE occurence of the observed natural disasters, such as earthquakes and tsunamis, appears to have increased in recent decades [1]. Quick observation of the damage caused by an earthquake and tsunami is extremely important for planning effective rescue operations. To understand the destruction situation over huge areas in a short time, airborne and spaceborne remote sensing is the most important and useful method. Airborne remote sensors are more flexible to monitor a specific area intensively with fine resolution. However, usually they suffer from the lack of corresponding before-event acquisitions. Spaceborne remote sensors have the advantage of covering a large imaging scene at one time. In addition, the regular orbit of the satellite enables it to revisit areas and to accumulate image archives that allow the comparison of before- and after-event observations. From these multitemporal images, the changes caused by the disaster can be understood and detected. To motivate further studies of damage assessment using remote sensing data, a large number of remote sensing data sets have been collected and placed on the website [2] for easy access.

High-resolution optical images which allow direct interpretation of the damages are usually used to investigate the impact of an event [3], [4]. Many change detection methods are available for optical images [5], [6], and the effects of residual misregistration of multitemporal images on change detection have been also studied [7]. However, the use of optical sensors for monitoring damaged areas is limited by cloudy weather and nighttime darkness. In contrast to optical sensors, synthetic aperture radar (SAR) as a microwave sensor can work day and night and is nearly unaffected by weather and atmospheric conditions. SAR images are particularly useful when weather conditions are not suitable for optical sensing. Several studies using multitemporal SAR images for earthquake damage evaluation have been reported [8]–[14]. Image pixel intensity changes and correlations have been intensively studied to understand and discriminate damage to urban areas [8]–[11]. When the temporal and spatial baselines are adequate to generate the interferometric SAR (InSAR) mode, the complex coherence of the interferometric pair can be another important source to understand the damage condition [12]. Multi-aspect SAR images have also been used for building damage evaluation [13], and a split-based approach has been reported for large-size SAR images for tsunami damage assessment [14]. The combination of optical and SAR image analysis methods has also been proposed for damage analysis [15]–[17].

However, due to the lack of data sets, limited work has been reported [18], [19] using full polarimetric SAR (PolSAR) images to examine the scattering mechanism changes caused by the natural disaster. Generally, full polarimetric techniques can better assist the understanding of scattering mechanisms and provide additional and more accurate information compared to single or partial polarization modes [20]. The superiority of the full polarimetric radar techniques have been demonstrated by a number of applications [20], [21]. Complementary to previous studies on damage evaluation, we will focus on full PolSAR images to explore the potential of using polarimetric information for tsunami damage investigation over urban areas. The study case is the great tsunami induced by the earthquake of March 11th, 2011, which occurred beneath the Pacific off the northeastern coast of Japan. The epicenter was located at 38.297° N, 142.372° E and 30 km in depth [22]. It was the largest earthquake and tsunami ever experienced in this region. Tsunamis caused by the earthquake reached a height of up to 20 m height in many areas and seriously damaged or destroyed the countryside of the Northeast coastal areas. As of Feb 24th, 2012, the total death toll from the earthquake and tsunami stood at 15,853 people; 3282 people were still missing, and more than 128,000 buildings were completely destroyed [23]. Full PolSAR images acquired before and after the tsunami by the spaceborne Advanced Land Observing Satellite/Phased Array type L-band Synthetic Aperture Radar (ALOS/PALSAR) [24]–[28] are used for analysis. This work aims to find relationships between the polarimetric parameters and the damage level. First, the polarimetric scattering mechanism changes before and after the tsunami at the city block level are examined by utilizing polarimetric techniques. We then propose two polarimetric indicators for damage level indication.

The remainder of this paper is organized as follows. In Section II, the full PolSAR data representation and interpreting techniques are briefly reviewed. The scattering mechanisms in urban areas are introduced and the scattering mechanism changes observed after the tsunami are also analyzed. Section III describes the study area and the ALOS data sets used in the study. Section IV presents the damage investigation using polarimetric techniques with ALOS/PALSAR multitemporal PolSAR images. Two damage level indicators are developed and compared in Section V. Further discussions, conclusions and perspectives are given in Sections VI and VII.

II. Polarimetric Scattering Mechanisms and Polarization Orientation Angles in Built-Up Areas

A. PolSAR Data Representation

For PolSAR, the acquired full polarimetric information can form the scattering matrix

$$S = \begin{bmatrix} S_{HH} & S_{HV} \\ S_{VH} & S_{VV} \end{bmatrix} \tag{1}$$

where S_{HV} is the backscattered return from horizontal transmitting and vertical receiving polarizations. The other terms are similarly defined.

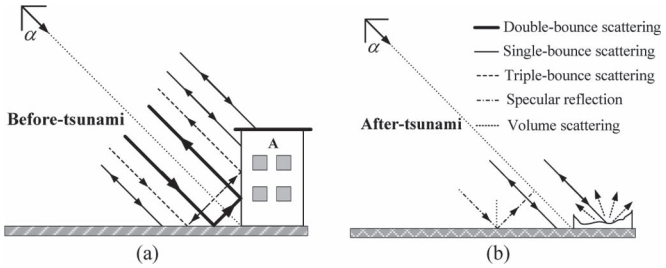

Fig. 1. Illustration of the changes of the polarimetric scattering mechanisms in a build-up area. (a) Before-tsunami. (b) After-tsunami.

Subject to the reciprocity condition ($S_{HV} \approx S_{VH}$), the commonly used coherency matrix T is generated

$$T = \left\langle k_P k_P^H \right\rangle = \begin{bmatrix} T_{11} & T_{12} & T_{13} \\ T_{21} & T_{22} & T_{23} \\ T_{31} & T_{32} & T_{33} \end{bmatrix} \tag{2}$$

where $\langle\ \rangle$ denotes the sample average, $k_P = [S_{HH} + S_{VV}\ S_{HH} - S_{VV}\ \sqrt{2}S_{HV}]^T$ is a Pauli scattering vector. k_P^H is the conjugate transpose of k_P, and T_{ij} is the (i, j) entry of T.

B. Scattering Mechanisms Investigation in Built-Up Area

For a built-up area without damage (e.g., before a tsunami), there are mainly three scattering components [29]. The illustration of these scattering mechanisms is shown in Fig. 1(a). The first contribution is the single-bounce scattering from ground surfaces, walls, or roofs. The second component is the double-bounce scattering formed by the ground-wall structures. The last mechanism is the triple-bounce scattering due to the ground-wall-ground and wall-ground-wall reflections. The dominant backscattering depends on the building orientation and the roughness of the surrounding terrain. As demonstrated in [29], if the surrounding surface is moderately rough, double-bounce scattering from the building is the dominant component of the electromagnetic return. In these cases, the triple-bounce scattering contribution is negligible compared with the double-bounce scattering component.

However, if the building A were flushed away during a tsunami, the scattering mechanisms would be significantly changed accordingly, as shown in Fig. 1(b). Changes of the scattering mechanisms are mainly determined by the changes of surface conditions. With the passage of time after the tsunami, the changes in surface condition before reconstruction can be classified as four cases.

Case i) The ground is flooded. This case happens during the tsunami and lasts a limited time after the tsunami. With the movement of the tsunami or significant wind and rain, flooded areas mainly exhibit surface scattering; otherwise, these areas generally appear dark due to specular reflection. A small amount of double-bounce or triple-bounce scattering could be observed from the interface of the water surface and any surviving buildings or debris that remained above the surface. However, since the debris is randomly oriented, this backscattering power could be

much lower than that observed over an intact urban area. Note that the situation of flood caused by a tsunami might be different from a flood due to heavy rain [30]. For the latter case, usually the buildings will not be flushed away and the building walls are still intact, so double-bounce scattering will be maintained by the water-wall structures.

Case ii) A large amount of debris has accumulated on the ground, but there is no open water. This situation can last a relatively long period after the flooded stage, and relates to the rescue, clean-up and reconstruction progress. The scattering phenomena in this case are very complicated. With different shapes, sizes, and orientations of the debris, the scattering mechanisms may significantly differ. This case can include all three of the scattering components that appear in normal urban areas. However, due to the destruction of the wall structures, the contribution of double-bounce scattering to the backscattered signal should be reduced. Moreover, if there are a number of elemental fragments which are small with respect to the wavelength of the incident wave, a small amount of volume scattering can be expected.

Case iii) A small or moderate amount of debris has accumulated on the ground. With the progress of the clean-up and reconstruction, debris has been cleared, especially those items that block roadways. Therefore, the main changes in the surface condition are an increase in surface roughness due to the remaining debris and an increase in the dielectric constant due to the increased soil moisture. Thereby, the surface scattering is enhanced while the double-bounce scattering is reduced accordingly.

Case iv) All the debris has been cleared. In this case, the main change is a consistent increase in the surface scattering.

In summary, for the above four stages of tsunami damage in an urban area, the main induced scattering mechanism change is that the double-bounce and triple-bounce scattering mechanisms will be reduced or vanish completely due to the destruction of the wall structures, and the signal will mainly change into one dominated by surface scattering. For the after-tsunami data sets (acquired on April 8th, 2011) used in this paper, the surface condition mainly belongs to the aforementioned cases ii and iii.

C. Polarimetric Scattering Models and Decomposition

To interpret the scattering mechanisms in the context of radar polarimetry, basic scattering models have been developed [20], [31], [32], and a brief review is given as follows.

1) Odd-Bounce Scattering Model: Both single-bounce and triple-bounce scattering show similar polarimetric signatures [33], and can be uniformly called odd-bounce scattering. The odd-bounce scattering model is represented by Bragg surface scattering phenomena from a slightly rough surface [20], [31]. The odd-bounce scattering model in coherency matrix formulation [34] is

$$T_{odd} = f_s \begin{bmatrix} 1 & \beta^* & 0 \\ \beta & |\beta|^2 & 0 \\ 0 & 0 & 0 \end{bmatrix} \tag{3}$$

where β relates to the reflection coefficients for horizontally and vertically polarized waves [20], [34].

2) Double-Bounce Scattering Model: The double-bounce scattering component is modeled by scattering from a dihedral corner reflector, such as ground-wall scatterer, where the reflector surfaces can be made of different dielectric materials [20], [31]. The double-bounce scattering mechanism in coherency matrix formulation [34] is

$$T_{dbl} = f_d \begin{bmatrix} |\alpha|^2 & \alpha & 0 \\ \alpha^* & 1 & 0 \\ 0 & 0 & 0 \end{bmatrix} \tag{4}$$

where α relates to the reflection coefficients for horizontally and vertically polarized waves from the ground and vertical surfaces [20], [34].

3) Volume Scattering Model: Volume scattering is usually modeled by a cloud of oriented elemental scatterers. The coherency matrix for volume scattering is obtained by the integration with a probability density function (PDF) $p(\theta)$ for scatterer orientation θ, and can be generally expressed as

$$\langle T_{vol} \rangle = \int_0^{2\pi} T(\theta) p(\theta) d\theta = \begin{bmatrix} a & d & e \\ d^* & b & f \\ e^* & f^* & c \end{bmatrix}. \tag{5}$$

With the predefined elemental scatterer structures (e.g., oriented thin dipole) and PDFs, many models are available with different assumptions [31], [32], [35]–[37]. As also pointed out in [37], there is no fundamental reason to prefer one characterization over another, and several empirical models have also been proposed in [38]–[40] as alternatives.

4) Model-Based Decomposition: Polarimetric model-based decomposition is an effective technique for better understanding the scattering mechanisms of PolSAR images [20]. A number of model-based decomposition methods have been developed [20], [31], [32], [34], [35], [37]–[42], and they have been successfully applied in many fields [43]–[46]. The general principle is to decompose one polarimetric matrix into a summation of several basic scattering models. Using the coherency matrix as an example, the form is

$$T = f_d T_{dbl} + f_v T_{vol} + f_s T_{odd} + \cdots \tag{6}$$

where T is the measured data; T_{dbl}, T_{vol}, and T_{odd} are, respectively, the double-bounce, volume and odd-bounce scattering models; and f_d, f_v, and f_s are the corresponding decomposed coefficients.

After the decomposition, the decomposed powers for each scattering mechanism are available, represented by P_d, P_v, and P_s for the double-bounce, volume and odd-bounce scattering mechanisms, respectively. The dominant scattering mechanism

for each resolution cell can be determined by comparing the relative values among P_d, P_v, and P_s.

The commonly used odd-bounce and double-bounce scattering models are shown in (3) and (4). In this paper, we adopt the recently improved Yamaguchi decomposition [41] for investigation, in which the volume scattering models are

$$T_{vol1} = \begin{bmatrix} 2 & 0 & 0 \\ 0 & 1 & 0 \\ 0 & 0 & 1 \end{bmatrix}$$

$$T_{vol2} = \begin{bmatrix} 15 & 5 & 0 \\ 5 & 7 & 0 \\ 0 & 0 & 8 \end{bmatrix}$$

$$T_{vol3} = \begin{bmatrix} 15 & -5 & 0 \\ -5 & 7 & 0 \\ 0 & 0 & 8 \end{bmatrix}. \quad (7)$$

The selection of each volume scattering model is determined by the ratio of the co-polarization powers, discussed in [32], [41].

D. Polarization Orientation Angle Investigation

Using the geometric descriptor of the polarization ellipse, the polarization state of an electromagnetic wave can be characterized by its polarization orientation (PO) angle θ and ellipticity angle τ [20], [47], shown in Fig. 2(a). In urban areas, the PO angle is highly correlated to the orientations of buildings [48], [49]. The scattering from an urban area is relatively deterministic and so are the measured PO angles. As a result, the shifted PO angles are relatively deterministic. For buildings parallel to the flight pass, the PO angle is zero, while oriented buildings will rotate the polarization basis and induce a PO angle shift from zero. Furthermore, for built-up areas with large orientation angles, the fluctuation of the estimated PO angle would increase. For damaged built-up areas, the scattering from surviving buildings and remaining foundations can be also deterministic. However, the scattering from the randomly oriented debris becomes less or non deterministic. The induced PO angles from such debris will also distribute randomly and the fluctuation can be significantly increased. Consequently, exploring the difference of the PO angle distributions before and after the tsunami has the potential to reflect the damage condition.

The PO angle was originally derived using a circular polarization method [47]. It can be verified that this method is equivalent to deorientation processing [50] which aims at minimizing the cross-polarization term by rotating the coherency matrix. The rotation angle [51], [52] is

$$\theta = \frac{1}{4}\left(\tan^{-1}\frac{2\mathrm{Re}(T_{23})}{T_{22}-T_{33}} \pm n\pi\right) \quad n = 0, 1. \quad (8)$$

The unwrapping factor $\pm n\pi$ is necessary; otherwise, the coherency matrix will be rotated toward the wrong axis and T_{33} will be incorrectly maximized [51], [52].

After the deorientation processing, the cross-polarization power T_{33} is minimized. Since oriented buildings will rotate the polarization basis, induce significant cross-polarization power, and cause scattering mechanism ambiguity, deorientation processing [50] has been adopted in model-based decomposition for PolSAR image interpretation [39], [41].

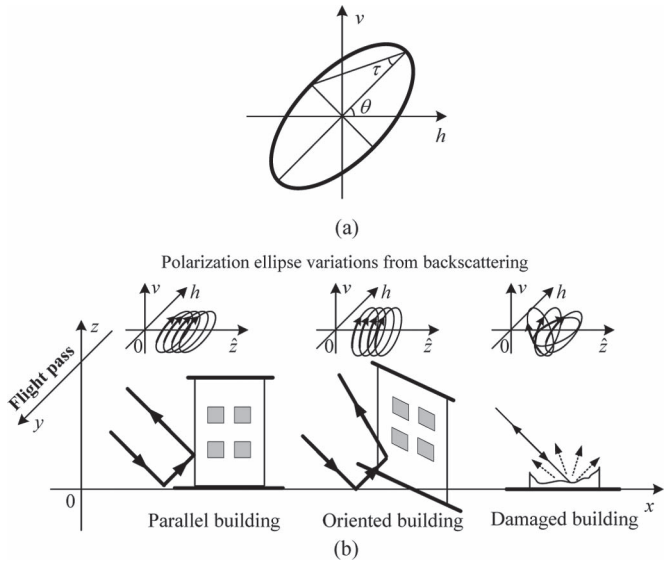

Fig. 2. (a) Polarization ellipse. (b) Illustration of the PO angle changes in a built-up area for parallel, oriented, and damaged buildings. $\hat{z}$ is the electromagnetic wave propagation direction.

III. ALOS Data and Study Area Description

The great tsunami caused by the March 11th earthquake struck the coast of Northeast Japan and caused significant damage. Most of the serious destruction occurred in villages that face the ocean and have steep mountains behind them. Although some villages had 10 m high sea walls, the great March 11th tsunami reached higher than 20 m in many locations, causing serious damage in these areas. The seriously damaged regions around the city of Ishinomaki, Miyagi prefecture [53] are selected for study. Most of the houses were completely washed away. The building damage map [54] is shown in Fig. 3(a).

Quick observations have been carried out using the ALOS satellite remote sensors. Until its mission was terminated on April 22th, 2011, ALOS had operated for 62 orbits and collected 643 scenes of the March 11th disaster from the onboard optical and SAR sensors [24]. During the ALOS lifetime, it has acquired five PolSAR data sets covering the study area of Ishinomaki city. The acquisition information is summarized in Table I. The local weather information [55] at the time closest to the radar acquisition is also included. There was no rainfall during the 12 hours before these five acquisitions [55]. There are four before-tsunami and one after-tsunami full polarimetric acquisitions. The minimum revisit cycle for ALOS is 46 days. The only full polarimetric data set collected after the tsunami was acquired on April 8th, 2011, while the latest before-tsunami data set was acquired on November 21st, 2010; the earliest before-tsunami data set was acquired on March 28th, 2007. From these data sets, four after- and before-tsunami pairs and six before-tsunami pairs can be generated. The temporal and spatial baselines for these multitemporal pairs are shown in Table II. The pairs are sorted in ascending order of the temporal

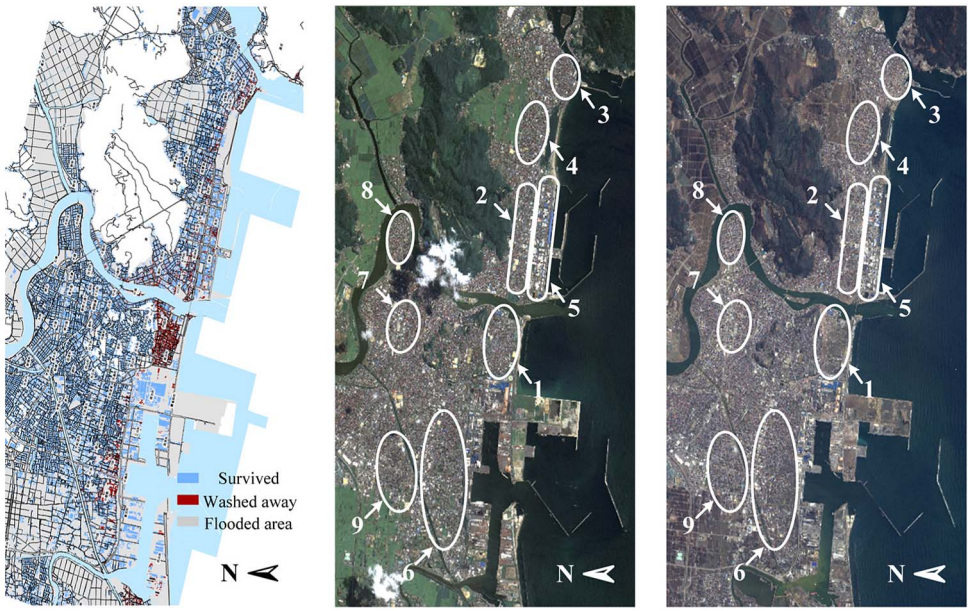

Fig. 3. Study area, covering about 10 km × 5 km and including the seriously damaged city of Ishinomaki, Miyagi, Japan. (a) Building damage map. Copyright 2011 ZENRIN CO., LTD. (b) and (c) are pan-sharpened true-color images generated from ALOS PRISM and AVNIR-2 data sets. (b) Before-tsunami (August 23rd, 2010). (c) After-tsunami (April 10th, 2011) images. Nine built-up patches are selected and numbered. The building damage levels for patch 1, patches 2 and 3, patches 4, 5, and 6, patches 7, 8, and 9 are 80–100%, 50–80%, 20–50% and 0–20%, respectively. The damage level is defined as the percentage of the buildings which were flushed away in one built-up patch and is estimated from the damage map.

TABLE I
ACQUISITION INFORMATION OF THE MULTITEMPORAL ALOS/PALSAR FULL POLARIMETRIC IMAGES OVER ISHINOMAKI CITY, MIYAGI. THE CORRESPONDING LOCAL WEATHER INFORMATION IS CITED FROM JAPAN METEOROLOGICAL AGENCY

Image No.	Acquisition date	Incidence angle (deg)	Wind speed (m/s)	Temperature (℃)
D1	April 8th, 2011	23.832	2.8	10.5
D2	November 21st, 2010	23.796	2.1	14.0
D3	April 2nd, 2009	23.774	5.8	4.6
D4	May 13th, 2007	23.773	7.5	13.9
D5	March 28th, 2007	23.780	1.3	5.8

TABLE II
BASELINE INFORMATION OF THE MULTITEMPORAL ALOS/PALSAR POLSAR IMAGE PAIRS

Multi-temporal pair	Temporal baseline (day)	Spatial baseline (m)
D1-D2	138	1747
D1-D3	736	4680
D1-D4	1426	3343
D1-D5	1472	3610
D4-D5	46	267
D2-D3	598	2932
D3-D4	690	1334
D3-D5	736	1069
D2-D4	1288	1595
D2-D5	1334	1862

baselines: the first four lines are the after- and before-tsunami data pairs, while the remainder of the table shows before-tsunami data pairs. For after- and before-tsunami pairs, the shortest temporal and spatial baselines are 138 days and 1747 meters, respectively. Such large baselines induce significant decorrelation effect and produce poor interferometric coherence. Thus, the PolInSAR mode [56] is not effective for these pairs.

The resolutions for the single-look ALOS/PALSAR PolSAR image are 4.45 m in the azimuth direction and 23.14 m in the ground-range direction at the imaging scene center [28]. The multiple images have been coregistered. 8-look multilooking processing in azimuth direction was implemented to adjust the azimuth and range pixel size to be comparable. The ALOS optical data sets were also coregistered to the PolSAR images for illustration. Pan-sharpened true-color image with 2.5m resolution, generated from ALOS Panchromatic Remote-Sensing Instrument for Stereo Mapping (PRISM), and the Advanced Visible and Near Infrared Radiometer type 2 (AVNIR-2) Level 1B2 data sets [57] observed on August 23rd, 2010 and April 10th, 2011, are used to show the damage condition. The corresponding ALOS optical images are shown in Fig. 3(b) and (c).

The resolution of the ALOS/PALSAR full PolSAR data is not fine enough to identify each building independently. Therefore, the scattering mechanism changes over the damaged urban areas are carried out at the city block scale. To find relationships between scattering mechanism changes and damage levels, nine built-up patches with dense buildings inside but different damage levels are manually delineated. These patches are highlighted in Fig. 3 with ellipse boxes and are numbered from 1 to 9. The damage level is defined as the percentage of the buildings which were flushed away in one built-up patch and is calculated from the damage map in Fig. 3(a). The damage level is divided into four groups: 80–100% (patch 1), 50–80% (patches 2 and 3), 20–50% (patches 4, 5, and 6), and 0%–20% (patches 7, 8, and 9). Higher damage level relates to a more seriously damaged area. However, note that 0%

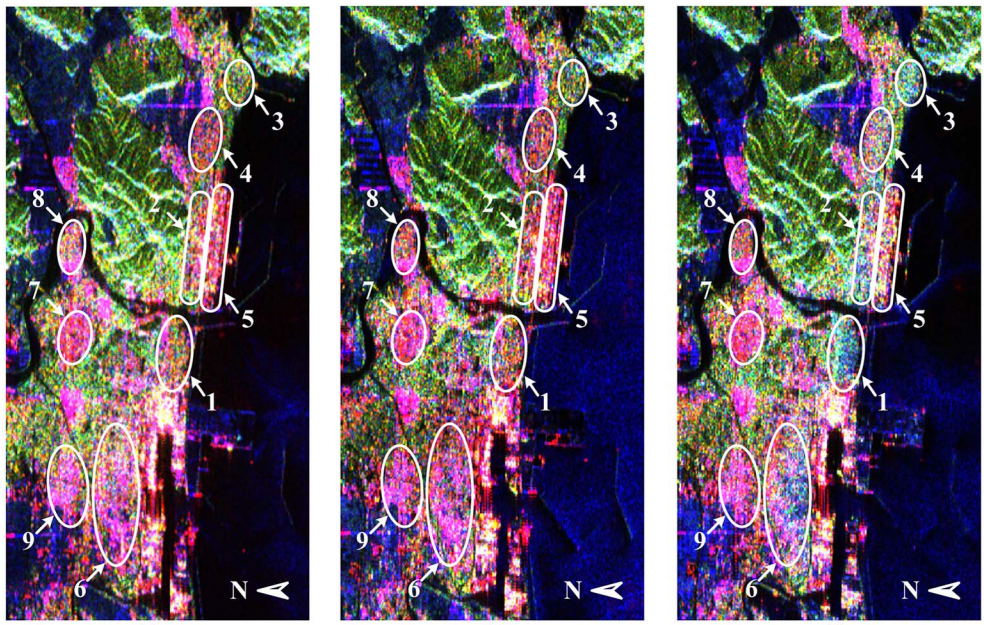

Fig. 4. Decomposition results of ALOS/PALSAR full polarimetric SAR data sets. (a) is the earliest before-tsunami image (D5), (b) is the latest before-tsunami image (D2), and (c) is the after-tsunami image (D1). The images are colored by P_d (red), P_v (green), and P_s (blue).

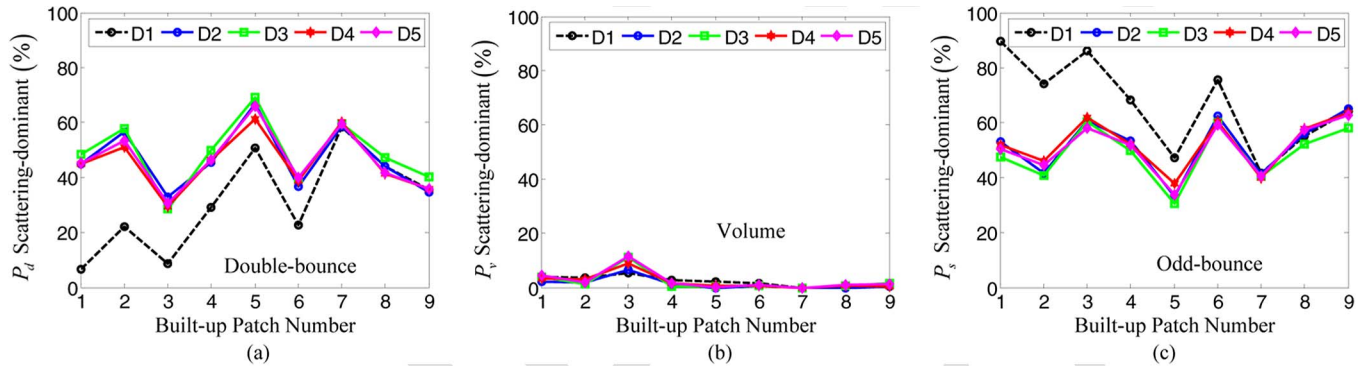

Fig. 5. Comparison of Yamaguchi decomposition before- and after-tsunami, for the built-up patches 1-9. (a)–(c) are comparisons of the double-bounce P_d, volume P_v and odd-bounce P_s scattering-dominant percentages, respectively.

damage level means that no buildings were washed away in that patch rather than truly no damage, since all these built-up areas were flooded during the tsunami and some damage was inevitable. Note also that although patch 2 is located farther from the ocean than patch 5, its damage level is higher than that of patch 5. The reason is that patch 5 contained mainly large industrial buildings, while patch 2 contained smaller and more numerous residential houses. When the tsunami came, the smaller wooden houses were more easily washed away than the concrete buildings.

IV. Damage Investigation Using Polarimetric Techniques

A. Polarimetric Scattering Mechanisms Examination

The recently developed Yamaguchi decomposition [41] which incorporates deorientation processing is used to understand the ground surface conditions and investigate the tsunami damage. Yamaguchi decomposition is applied with rotated coherency matrices. Due to the coarse resolution, to keep all the image details, the speckle filtering [58], [59] has not been used, and this consideration is the same as [41]. The deorientation processing by rotating the coherency matrix is used to minimize the cross-polarization term. Decomposition results from the earliest and latest before-tsunami, and after-tsunami data sets are displayed in Fig. 4. On the whole, in the before-tsunami images, the built-up areas are dominated by the double-bounce scattering mechanism, the mountainous areas covered with forests are dominated by the volume scattering mechanism and the ocean areas clearly show a dominance of the surface scattering mechanism. These observations can also be obtained from the other two before-tsunami data sets. However, after the tsunami, it is observed from the corresponding damage map and optical images, shown in Fig. 3, that most of the houses near the seashore were washed away completely, leaving a relatively rough surface. Therefore, it is clear that from the decomposition results, the dominant scattering mechanism of the heavily damaged built-up regions changed from double-bounce scattering (red) to odd-bounce scattering (blue).

Furthermore, the selected nine built-up patches with varying damage levels are used for further quantitative comparison. The scattering power contributions are examined for these built-up patches. Fig. 5 shows the results of decomposition comparison; the three plots respectively give the percentage contributions of the double-bounce P_d, volume P_v, and odd-bounce P_s scattering-dominant mechanisms for the five PolSAR images. Due to the tsunami, the contributions of the double-bounce scattering-dominant mechanism consistently dropped for the damaged patches 1–6 where a portion of the buildings were flushed away. Meanwhile, the contributions of the odd-bounce scattering-dominant increased accordingly. The contributions of volume scattering-dominant mechanism remained almost the same as before, and only a slight increase is observed, which could have been induced by backscattering from the remaining small debris which were randomly oriented. Therefore, the majority of the reduction in double-bounce scattering-dominant was due to it changing into odd-bounce scattering-dominant which theoretically indicates rough surface terrain. In addition, for patches 7–9 where almost no buildings were washed away, the scattering mechanisms remained about the same as the before the tsunami. Comparisons of the four before-tsunami results clearly demonstrate that the dominant scattering contributions showed almost no changes for all these built-up patches; only slight fluctuations are observed. Considering the temporal and spatial baselines shown in Table II, the local terrains could have exhibited some changes during the duration of the two acquisitions. In addition, the built-up patches are manually delineated without any building mask. The included pixels from vegetation areas may also degrade the correlation and affect the final result. Therefore, these small fluctuations are acceptable and explainable. Compared with the changes induced by the tsunami damage, these fluctuations are negligible.

As a summary, for before-tsunami results, the dominant scattering contributions remained the same relative to each other for all patches. After the tsunami, the double-bounce scattering-dominant contribution was significantly reduced and mainly changed into odd-bounce scattering-dominant component for the damaged patches, while the scattering mechanisms for undamaged patches remained relatively no change. These observations can be interpreted in light of the fact that the ground-wall dihedral structures were significantly decreased due to the equivalent amount of buildings which were washed away. These polarimetric scattering mechanism examinations agree well with both the theoretical analysis in Section II-B and the visual judgment from the optical images. Furthermore, comparisons from these multitemporal data sets also validate the idea that the ground-wall dihedral structures in built-up areas can be permanent and stable even over a long temporal baseline [60]. This is also supported by the permanent scatterer detection principle [61]. Therefore, we further explore this characteristic for damage level characterization in the next section.

B. Polarization Orientation Angle Shift Examination

As have been demonstrated in [48], [49], PO angles have a close relationship to the orientations of the buildings themselves. Usually, buildings or houses in one built-up block or unit are regularly located and have similar orientation angles. The estimated PO angles should clearly reflect this phenomenon and be homogeneously distributed. However, after the earthquake and tsunami, many buildings were collapsed and most of them were washed away near the seashore. The regularity of these buildings was significantly destroyed and a large amount of randomly oriented debris was produced. Strong reflections from debris and the remaining building bases may reduce the homogeneity of the PO angle distribution. Therefore, the comparison of the PO angles in a built-up patch where the buildings are aligned in similar orientations, before and after the damage, can provide useful information to assist damage understanding. In addition, the local incidence angles, shown in Table I, are very close to each other and their impact on PO angle comparison is neglected.

The PO angles are calculated for comparison, shown in Fig. 6 for the study area before and after the tsunami. The earliest and latest before-tsunami data sets are displayed. The selected nine built-up patches in the last subsection are also highlighted accordingly. From the optical images in Fig. 3, the buildings in each patch were uniformly distributed with similar orientations before the tsunami, where the PO angles from Fig. 6 are homogeneous for these built-up patches. However, after the tsunami, portions of the buildings were flushed away and the land cover conditions were significantly changed. The uniform orientations of these buildings were broken. Furthermore, the strong reflections from the remaining randomly oriented debris may have induced random PO angles, while the reflections from the foundations of the washed-away buildings may be associated with deterministic orientation angles. Therefore, the distribution of PO angles from after the tsunami spreads to a wider range with much higher fluctuation than that before the tsunami. To demonstrate these analyses, histograms of the PO angles from before and after the tsunami of built-up patches 1, 3, 5, and 7 (one patch from each damage level) are shown in Fig. 7. From Figs. 6 and 7, before-tsunami PO angles were more homogeneous than those after the tsunami, especially for heavily damaged patches 1 and 3. The majority of before-tsunami PO angles fall within a narrow range, while those from after the tsunami spread to a larger range, up to the full range. For patch 7, the PO angle distributions for both before- and after-tsunami are very similar. In addition, PO angles from a built-up patch with large orientation angles could also spread to a larger range, even the full range such as in patches 1 and 3. However, the distribution shapes are obviously different between the before- and after-tsunami pair while they are similar for the before-tsunami pairs.

Therefore, although the PolSAR image resolution is not fine enough to resolve individual buildings, at the city block scale the relationship between the homogeneity of the estimated PO angles and the built-up patch with similar oriented buildings inside is clearly demonstrated. If most of the buildings in a patch survived the tsunami (as in patches 7–9), the homogeneity of the corresponding PO angles remains. On the other hand, if the built-up patch is seriously damaged, the corresponding PO angles become less homogeneous (e.g., in patches 2–6) even heterogeneous (patch 1). Therefore, the changes of the PO angle distributions before- and after-tsunami can

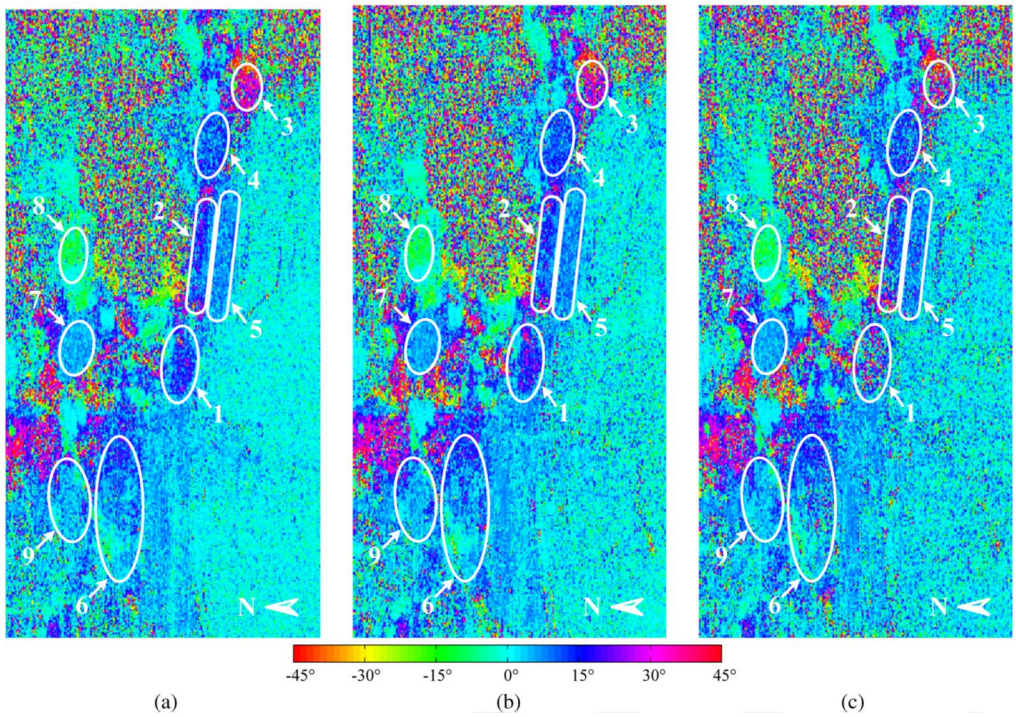

Fig. 6. Estimated PO angle images. (a) is the earliest before-tsunami image (D5), (b) is the latest before-tsunami image (D2), and (c) is the after-tsunami image (D1).

be useful for damage evaluation. Quantitative characterization of the damage effect using PO angle is developed in the following section.

V. Damage Level Characterization

When interferometry is not available, the intensity correlation is commonly used for damage level indication [8]–[11]. However, the intensity values can be easily changed among long temporal baseline PolSAR images without any natural disaster, due to the stochastic nature of the decorrelation effect. As a comparison, basic scattering structures such as the ground-wall dihedral structures in built-up areas are more permanent and stable even over a long temporal baseline. Therefore, damage level indexes developed from the polarimetric scattering mechanism analysis techniques can be more robust than those based on intensity changes. Two indicators from the model-based decomposition and PO angle analysis are developed and examined in the following.

A. Ratio of the Double-Bounce Scattering-Dominant Contributions

The great tsunami flushed away a large number of buildings near the coastline. The damage level used in this paper is determined by the fraction of flushed away buildings in a local built-up patch. This reduction in the number of intact buildings may produce an equivalent reduction in the amount of ground-wall dihedral structures. Since the double-bounce scattering in urban areas directly relates to the ground-wall dihedral structures, the ratio of the double-bounce scattering-dominant contributions after- and before-tsunami can reflect the same decreasing trend. This is the physical background of the following analysis. As discussed in Section II, the percentages of the dominant scattering mechanisms in each built-up patch can be obtained with model-based decomposition. Therefore, the reduced double-bounce scattering-dominant mechanism directly relates to the destroyed ground-wall structures. The ratio of the double-bounce scattering-dominant contributions after- and before-tsunami is proposed as the first index for the damage level assessment

$$\text{Ratio}_{(\text{D}n-\text{D}m,i)} = \frac{(\text{Dominant } P_d)_{(\text{D}n,i)}}{(\text{Dominant } P_d)_{(\text{D}m,i)}} \tag{9}$$

where i is the built-up patch number and $i = 1, 2, \ldots, 9$. $\text{D}n - \text{D}m$ is one multitemporal pair. For after- and before-tsunami pairs, $\text{D}n = \text{D1}$.

Ratio values from after- and before-tsunami pairs for each selected built-up patch are shown in Fig. 8(a). The temporal baselines vary from 138 days to 1472 days, while the spatial baselines vary from 1747 m to 4680 m. For all these configurations, the linear relationship between this ratio index and the damage level is very clear: the ratio drops with increasing degree of damage. The damage level for patch 1 is 80–100% which means an equivalent fraction of ground-wall structures were destroyed and the corresponding ratios of the dominant P_d between after- and before-tsunami are within 0–0.2. The ratios are within 0.2–0.5 for patches 2 and 3 where the damage level is 50–80%, while it is within 0.5–0.8 for patches 4–6 where the damage level is 20–50%. Furthermore, for patches 7–9 where almost no buildings were washed away, the ratios are around 1. Only the ratio of patch 5 from the D1-D4 pair is slightly over 0.8, and $\text{Ratio}_{(\text{D1}-\text{D4},5)} = 0.825$. Even so, this ratio is smaller than the smallest ratio value from patches 7–9 where the smallest value is $\text{Ratio}_{(\text{D1}-\text{D3},9)} = 0.886$. While

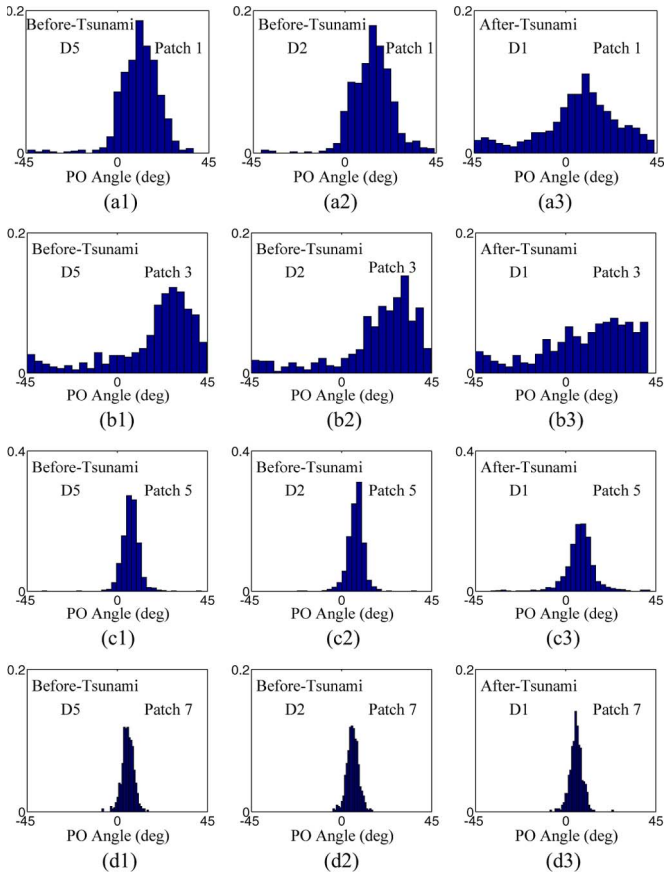

Fig. 7. Histograms of the PO angles for built-up patches 1, 3, 5, and 7 with damage levels 80–100%, 50–80%, 20–50%, and 0–20%, respectively. (a1)–(d1) are the earliest before-tsunami (D5), (a2)–(d2) are the latest before-tsunami (D2), (a3)–(d3) are the after-tsunami (D1), respectively.

slight fluctuations can be observed among these multitemporal pairs, no obvious tendency is observed in the temporal or spatial baseline dependence.

For further validation, ratio values from before-tsunami pairs for each selected built-up patch are also compared and shown in Fig. 8(b). The temporal baselines vary from 46 days to 1334 days, while the spatial baselines vary from 267 m to 2932 m. For selected built-up patches, the ratios from these multitemporal pairs are all around 1. The largest ratio value is $\text{Ratio}_{(\text{D2}-\text{D3},3)} = 1.152$, and the smallest ratio value is $\text{Ratio}_{(\text{D2}-\text{D3},9)} = 0.866$. This evidence validates the stability of the ground-wall permanent structures and the resulting double-bounce scattering mechanism in an urban area. Therefore, the ratio of the reduced double-bounce scattering-dominant mechanism effectively reflects the reduced ground-wall structures, and can be used for damage level indication.

B. Standard Deviation of PO Angle Differences

As aforementioned, PO angle is an intrinsic parameter of electromagnetic waves, and is linked to the orientations of buildings. At the city block scale, buildings usually have similar orientations. However, after the tsunami, some of the buildings were flushed away, leaving a number of building foundations and much debris. Some randomly oriented debris could produce strong reflections together with the randomly distributed PO

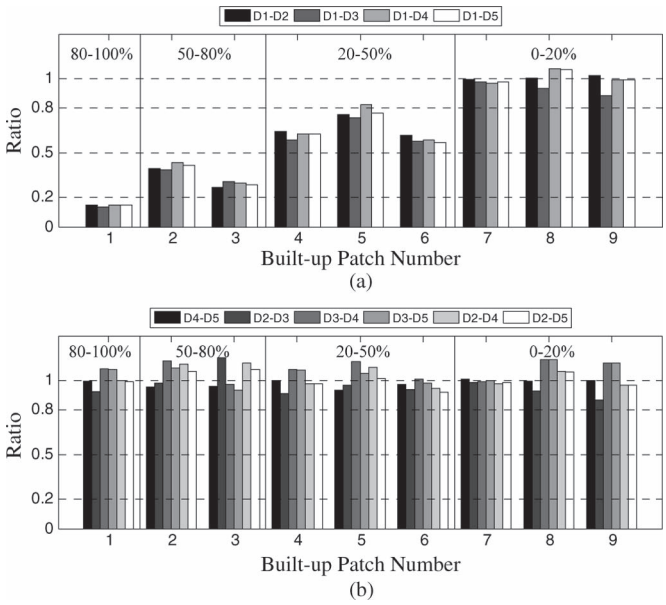

Fig. 8. Ratios of the double-bounce scattering-dominant contributions for the selected built-up patches. (a) After- and before-tsunami pairs. (b) Before-tsunami pairs.

angles. Therefore, the homogeneity of the PO angle in a block is reduced with increasing damage level.

The PO angle sequences without sorting are shown in Figs. 9(a)–(d) for patches 1, 3, 5, and 7, respectively. From these figures, the differences between before- and after-tsunami are not clear due to the high fluctuation pixel by pixel. However, inspired by the corresponding PO angle histograms shown in Fig. 7, the rearranged PO angle sequences sorted in descending order are shown in Figs. 9(e)–(h). The PO angle differences between before- and after-tsunami become obvious. With increasing damage level, the PO angle differences are also enhanced. For patch 7, the PO angle sequences are well overlapped. Furthermore, the PO angle sequences from the earliest and latest before-tsunami acquisitions D5 and D2 are very similar for all these patches. To characterize the changes of the PO angle distributions from one multitemporal pair, the standard deviation of the differences of two sorted PO angle sequences is proposed as another damage level indicator

$$\text{Std}_{(\text{D}n-\text{D}m,i)} = \left| std\left(\{\theta_p\}_{(\text{D}n,i)} - \{\theta_q\}_{(\text{D}m,i)} \right) \right| \qquad (10)$$

where $\{\theta_p\}_{(\text{D}n,i)}$ is the PO angle sequence sorted in descending order. $std(\cdot)$ is used to obtain the standard deviation, while $|\cdot|$ is to get the absolute value.

The index $\text{Std}_{(\text{D}n-\text{D}m,i)}$ obtained from standard deviation can also account for the fact that PO angle distribution from a built-up patch with large dominant orientation spreads to a larger range than that from a built-up patch with a smaller dominant orientation.

The index values from after- and before-tsunami pairs for each selected built-up patch are shown in Fig. 10(a). For all these various temporal and spatial baselines combinations, the trend is clear that with increasing damage level the $\text{Std}_{(\text{D}n-\text{D}m,i)}$ values also increase accordingly. The standard deviation is around or over 10° for patch 1 and is within $4^\circ - 8^\circ$

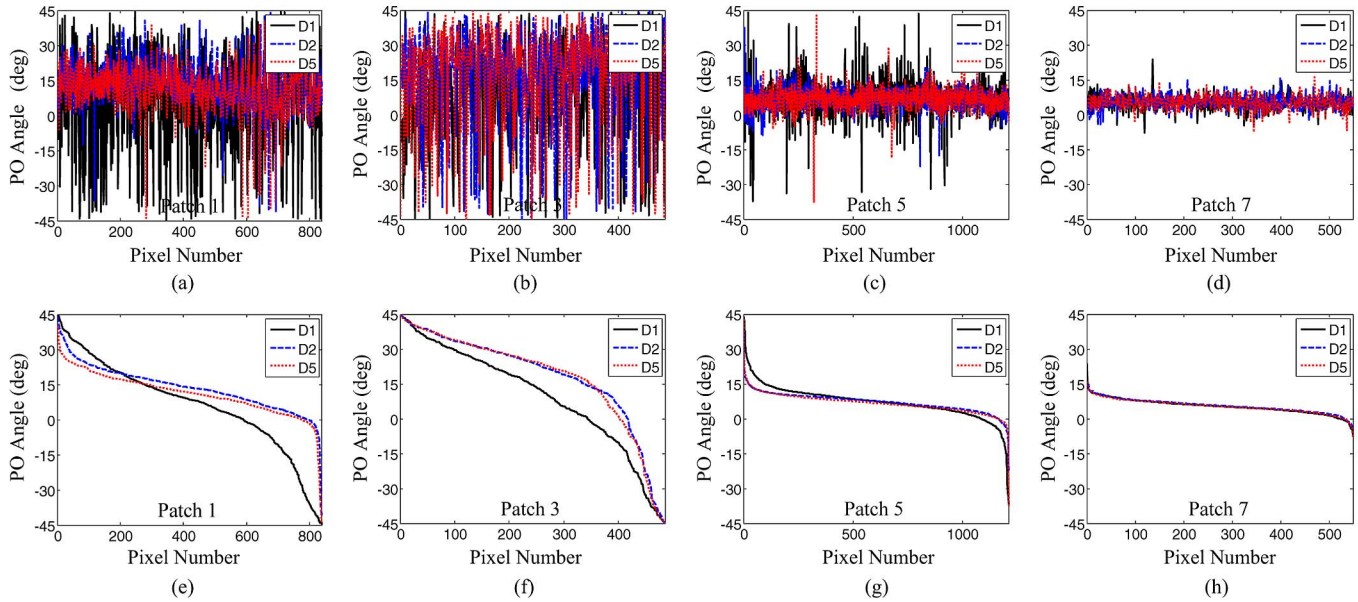

Fig. 9. PO angle sequences of D1, D2 and D5 acquisitions, for built-up patches 1, 3, 5, and 7. (a)–(d) are without sorting. (e)–(h) are sorted in descending order.

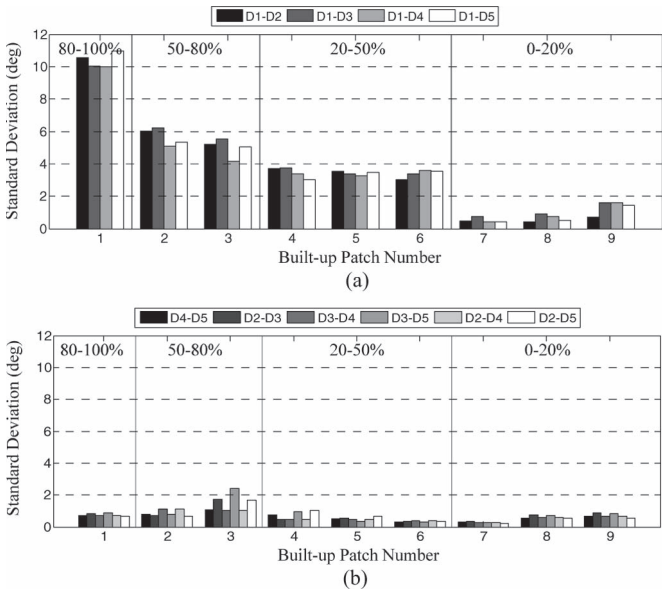

Fig. 10. Standard deviations (in deg) of PO angle differences after- and before-tsunami, for the selected built-up patches. (a) After- and before-tsunami pairs, (b) Before-tsunami pairs.

for patches 2 and 3. For less damaged patches 4–6, the standard deviation is within $2^\circ - 4^\circ$, while for patches 7–9, it is below 2°. Therefore, at the block scale, comparisons of the PO angle distributions provide valuable information for understanding damage conditions.

For further validation, $\mathrm{Std}_{(\mathrm{D}n-\mathrm{D}m,i)}$ values from before-tsunami pairs are also calculated and are shown in Fig. 10(b). For selected built-up patches, the standard deviations from these multitemporal pairs are almost below 2°. The only exception is from the D3–D5 pair over patch 3, where $\mathrm{Std}_{(\mathrm{D3}-\mathrm{D5},3)} = 2.411^\circ$. However, it is still much less than the smallest value from after- and before-tsunami pairs over damaged patches where the smallest value is $\mathrm{Std}_{(\mathrm{D1}-\mathrm{D5},4)} = 3.021^\circ$. Therefore, using $\mathrm{Std}_{(\mathrm{D}n-\mathrm{D}m,i)}$ can be effective to discriminate the built-up patches with different damage levels. These investigations also confirm the efficiency and the stability of the PO angle distributions in urban area.

VI. Discussion

A. Model-Based Decomposition Selection

Polarimetric model-based decompositions are commonly used for PolSAR image interpretation [20]. Due to the overestimation of volume scattering contributions and the scattering mechanism ambiguity between forests and oriented buildings, model-based decomposition has received more attention recently, and many advancements have been reported [35], [37], [39], [40]–[42]. For example, deorientation processing [50] has been incorporated into model-based decomposition schemes to cure scattering mechanism ambiguity [39], [41]. The adopted Yamaguchi decomposition in this paper belongs to this category. Improved decomposition results can be obtained for terrains consisting of oriented buildings.

However, the volume scattering models in (7) are not fully adaptive. Some adaptive volume scattering models with other predefined elemental scatterers and PDFs have been proposed [35]–[37]. Therefore, these methods could also be suitable for damage investigation and are worth trying. Furthermore, the oriented buildings can rotate the polarization basis and induce significant cross-polarization power. Although deorientation processing minimizes the cross-polarization power along the radar line of sight, it can not fully compensate for the cross-polarization power induced by the azimuth tilts of an oriented building, since the ground-wall dihedral structure is oriented with the normal to the ground instead of the radar line of sight. Furthermore, the commonly used double-bounce scattering model (4) does not account for the facts that oriented buildings rotate the polarization basis and induce significant cross-polarization power. Therefore, extensions of the current scattering models or general models are also required to better

understand the scattering mechanism and damage condition [52], [62].

B. Remarks and Perspectives

Spaceborne ALOS/PALSAR full PolSAR images can provide large-scale monitoring and understanding of the damage area. However, its resolution is not fine enough to identify each building. Therefore, the investigations of the polarimetric scattering mechanism changes caused by the tsunami are carried out at city block scale. The comparisons of the changes of the double-bounce scattering-dominant mechanism and the standard deviation of the PO angle differences are under the condition that the revisit orbits are relatively close and parallel. Therefore, the differences of the local incidence angles between the multitemporal images are negligible. For large spatial baseline and multiple looking aspects cases, the differences of the local incidence angles should be considered. The formula including the local incident angle has been derived in [48], [49]. In addition, if the before- and after-event acquired data sets can be used to generate the PolInSAR mode, the PolInSAR complex coherence can be another interesting indicator for damage understanding and worth for investigation.

Although the built-up patches were manually delineated in this paper, with the advancement of unsupervised change detection algorithms, such as the split-based approach [14], and combing the derived polarimetric damage indexes, automatic damage detection for large-scale multitemporal PolSAR image is possible. Furthermore, for detailed information extraction, such as the damage degree characterization of each building [15], very high-resolution PolSAR images or optical images are necessary. While airborne SAR is more flexible to acquire data sets for specific areas, pre-event archive data sets are usually lacking. Therefore, joint analysis of large-scale spaceborne PolSAR images and fine-resolution airborne PolSAR images has the greater potential to fully understand the damage situation.

VII. Conclusion

This paper focuses on tsunami damage investigation over urban areas by exploring the multitemporal spaceborne ALOS/PALSAR PolSAR images. The polarimetric scattering mechanism changes before- and after-tsunami, at the city block scale, have been examined using model-based decomposition and PO angle techniques. These analyzes are used to establish the relationships between the polarimetric scattering mechanism changes and damage levels. The basic scattering structures such as ground-wall dihedral structures from the built-up areas were found to be stable even over a long temporal baseline. Therefore, damage level indexes developed from the polarimetric scattering mechanism analysis techniques are more robust. Two polarimetric indexes have been proposed for damage level indication. One is the ratio of dominant double-bounce scattering contributions after and before the tsunami, which reflects the amount of destroyed ground-wall structures. The second index is the standard deviation of the PO angle differences, which is used to interpret the PO angle homogeneity reduction in a block of buildings. Experimental results validate the efficiency and stability of these two indicators, since the built-up areas with different damage levels are well discriminated. These results demonstrate the importance and efficiency of full polarimetric information for natural disaster assessment.

Further efforts and investigations are needed to fully explore polarimetric information for damage understanding and evaluation over other land covers. Comparison studies of single-, dual-, and full-polarization on damage assessment will also be addressed in the near future. In addition, for practical application, other important research topics are the development of a robust damage detection algorithm and damage mapping technique combined with other GIS data sets. In addition, if fine resolution PolSAR data sets are available, more detailed evaluation could be expected.

Acknowledgment

The authors would like to thank Dr. M. Shimada and M. Ohki of the Japan Aerospace Exploration Agency (JAXA), Japan, for providing the valuable data sets from the ALOS satellite, Dr. Z. S. Zhou of Commonwealth Scientific and Industrial Research Organisation (CSIRO), Australia, for his valuable suggestions. The authors also thank the editors and anonymous reviewers for their constructive suggestions.

References

[1] P. Hoyois, J.-M. Scheuren, R. Below, and D. Guha-Sapir, "Annual disaster statistical review: Numbers and trends 2006," CRED, Brussels, Belgium, 2007, Tech. Rep.

[2] [Online]. Available: http://supersites.earthobservations.org/main.php

[3] M. Pesaresi, A. Gerhardinger, and F. Haag, "Rapid damage assessment of built-up structures using VHR satellite data in tsunami-affected areas," *Int. J. Remote Sens.*, vol. 28, no. 13/14, pp. 3013–3036, Jun. 2007.

[4] M. Turker and B. T. San, "Detection of collapsed buildings caused by the 1999 Izmit, Turkey earthquake through digital analysis of post-event aerial photographs," *Int. J. Remote Sens.*, vol. 25, no. 21, pp. 4701–4714, Nov. 2004.

[5] L. Bruzzone and D. F. Prieto, "Automatic analysis of the difference image for unsupervised change detection," *IEEE Trans. Geosci. Remote Sens.*, vol. 38, no. 3, pp. 1171–1182, May 2000.

[6] M. Dalla Mura, J. A. Benediktsson, F. Bovolo, and L. Bruzzone, "An unsupervised technique based on morphological filters for change detection in very high resolution images," *IEEE Geosci. Remote Sens. Lett.*, vol. 5, no. 3, pp. 433–437, Jul. 2008.

[7] F. Bovolo, L. Bruzzone, and S. Marchesi, "Analysis and adaptive estimation of the registration noise distribution in multitemporal VHR images," *IEEE Trans. Geosci. Remote Sens.*, vol. 47, no. 8, pp. 2658–2671, Aug. 2009.

[8] M. Matsuoka and F. Yamazaki, "Use of satellite SAR intensity imagery for detecting building areas damaged due to earthquakes," *Earthq. Spectra*, vol. 20, no. 3, pp. 975–994, 2004.

[9] C. Yonezawa and S. Takeuchi, "Decorrelation of SAR data by urban damages caused by the 1995 Hyogoken-Nambu earthquake," *Int. J. Remote Sens.*, vol. 22, no. 8, pp. 1585–1600, 2001.

[10] M. Matsuoka and F. Yamazaki, "Building damage mapping of the 2003 Bam, Iran, Earthquake using Envisat/ASAR intensity imagery," *Earthq. Spectra*, vol. 21, no. 81, pp. 8285–8294, 2005.

[11] M. Matsuoka, S. Koshimura, and N. Nojima, "Estimation of building damage ratio due to earthquakes and tsunamis using satellite SAR imagery," in *Proc. IEEE Int. Geosci. Remote Sens. Symp.*, Honolulu, HI, Jul. 2010, pp. 3347–3349.

[12] G. A. Arciniegas, W. Bijker, N. Kerle, and V. A. Tolpekin, "Coherence- and amplitude-based analysis of seismogenic damage in Bam, Iran, using ENVISAT ASAR data," *IEEE Trans. Geosci. Remote Sens.*, vol. 45, no. 6, pp. 1571–1581, Jun. 2007.

[13] T. Balz and M. S. Liao, "Building-damage detection using post-seismic high-resolution SAR satellite data," *Int. J. Remote Sens.*, vol. 31, no. 13, pp. 3369–3391, Apr. 2010.

[14] F. Bovolo and L. Bruzzone, "A split-based approach to unsupervised change detection in large-size multitemporal images: Application to tsunami-damage assessment," *IEEE Trans. Geosci. Remote Sens.*, vol. 45, no. 6, pp. 1658–1670, Jun. 2007.

[15] D. Brunner, G. Lemoine, and L. Bruzzone, "Earthquake damage assessment of buildings using VHR optical and SAR imagery," *IEEE Trans. Geosci. Remote Sens.*, vol. 48, no. 5, pp. 2403–2420, May 2010.

[16] M. Chini, N. Pierdicca, and W. J. Emery, "Exploiting SAR and VHR optical images to quantify damage caused by the 2003 Bam earthquake," *IEEE Trans. Geosci. Remote Sens.*, vol. 47, no. 1, pp. 145–152, Jan. 2009.

[17] P. Gamba, F. Dell'Acqua, and G. Trianni, "Rapid damage detection in the Bam area using multitemporal SAR and exploiting ancillary data," *IEEE Trans. Geosci. Remote Sens.*, vol. 45, no. 6, pp. 1582–1589, Jun. 2007.

[18] M. Sato, S. W. Chen, and M. Satake, "Polarimetric SAR analysis of tsunami damage following the March 11, 2011 East Japan earthquake," *Proc. IEEE*, vol. 100, pp. 2861–2875, Oct. 2012.

[19] M. Watanabe, T. Motohka, Y. Miyagi, C. Yonezawa, and M. Shimada, "Analysis of urban areas affected by the 2011 off the Pacific Coast of Tohoku earthquake and tsunami with L-band SAR full-polarimetric mode," *IEEE Geosci. Remote Sens. Lett.*, vol. 9, no. 3, pp. 472–476, May 2012.

[20] J. S. Lee and E. Pottier, *Polarimetric Radar Imaging: From Basics to Applications*. Boca Raton, FL: CRC Press, 2009.

[21] J. S. Lee, M. R. Grunes, and E. Pottier, "Quantitative comparison of classification capability: Fully polarimetric versus dual and single-polarization SAR," *IEEE Trans. Geosci. Remote Sens.*, vol. 39, no. 11, pp. 2343–2351, Nov. 2001.

[22] [Online]. Available: http://earthquake.usgs.gov/earthquakes/eqinthenews/2011/usc0001xgp/

[23] [Online]. Available: http://www.npa.go.jp/archive/keibi/biki/higaijokyo.pdf, (In Japanese)

[24] M. Shimada, M. Watanabe, M. Takahashi, T. Motooka, M. Ohki, T. Yamanokuchi, Y. Miyagi, N. Kawano, T. Shiraishi, and R. Thapa, "Monitoring the great east Japan earthquake using ALOS," *IEEE Geosci. Remote Sens. Soc. Newslett.*, pp. 19–24, Dec. 2011.

[25] M. Shimada, T. Tadono, and A. Rosenqvist, "Advanced Land Observing Satellite (ALOS) and monitoring global environmental change," *Proc. IEEE*, vol. 98, no. 5, pp. 780–799, May 2010.

[26] A. Rosenqvist, M. Shimada, N. Itoh, and M. Watanabe, "ALOS PALSAR: A pathfinder mission for global-scale monitoring of environment," *IEEE Trans. Geosci. Remote Sens.*, vol. 45, no. 11, pp. 3307–3316, Nov. 2007.

[27] M. Shimada, O. Isoguchi, T. Tadono, and K. Isono, "PALSAR radiometric and geometric calibration," *IEEE Trans. Geosci. Remote Sens.*, vol. 47, no. 12, pp. 3915–3932, Dec. 2009.

[28] [Online]. Available: http://www.eorc.jaxa.jp/ALOS/en/guide/topics.htm

[29] G. Franceschetti, A. Iodice, and D. Riccio, "A canonical problem in electromagnetic backscattering from buildings," *IEEE Trans. Geosci. Remote Sens.*, vol. 40, no. 8, pp. 1787–1801, Aug. 2002.

[30] D. C. Mason, R. Speck, B. Devereux, G. J. P. Schumann, J. C. Neal, and P. D. Bates, "Flood detection in urban areas using TerraSAR-X," *IEEE Trans. Geosci. Remote Sens.*, vol. 48, no. 2, pp. 882–894, Feb. 2010.

[31] A. Freeman and S. L. Durden, "A three-component scattering model for polarimetric SAR data," *IEEE Trans. Geosci. Remote Sens.*, vol. 36, no. 3, pp. 963–973, May 1998.

[32] Y. Yamaguchi, T. Moriyama, M. Ishido, and H. Yamada, "Four-component scattering model for polarimetric SAR image decomposition," *IEEE Trans. Geosci. Remote Sens.*, vol. 43, no. 8, pp. 1699–1706, Aug. 2005.

[33] J. S. Lee, E. Krogager, T. L. Ainsworth, and W. M. Boerner, "Polarimetric analysis of radar signature of a manmade structure," *IEEE Geosci. Remote Sens. Lett.*, vol. 3, no. 4, pp. 555–559, Oct. 2006.

[34] Y. Yamaguchi, Y. Yajima, and H. Yamada, "A four-component decomposition of POLSAR images based on the coherency matrix," *IEEE Geosci. Remote Sens. Lett.*, vol. 3, no. 3, pp. 292–296, Jul. 2006.

[35] M. Neumann, L. Ferro-Famil, and E. Pottier, "A general model-based polarimetric decomposition scheme for vegetated areas," in *Proc. POLinSAR Workshop*, Franscati, Italy, 2009.

[36] M. Arii, J. J. van Zyl, and Y. Kim, "A general characterization for polarimetric scattering from vegetation canopies," *IEEE Trans. Geosci. Remote Sens.*, vol. 48, no. 9, pp. 3349–3357, Sep. 2010.

[37] M. Arii, J. J. van Zyl, and Y. Kim, "Adaptive model-based decomposition of polarimetric SAR covariance matrices," *IEEE Trans. Geosci. Remote Sens.*, vol. 49, no. 3, pp. 1104–1113, Mar. 2011.

[38] A. Freeman, "Fitting a two-component scattering model to polarimetric SAR data from forests," *IEEE Trans. Geosci. Remote Sens.*, vol. 45, no. 8, pp. 2583–2592, Aug. 2007.

[39] W. T. An, Y. Cui, and J. Yang, "Three-component model-based decomposition for polarimetric SAR data," *IEEE Trans. Geosci. Remote Sens.*, vol. 48, no. 6, pp. 2732–2739, Jun. 2010.

[40] S. W. Chen and M. Sato, "Model-based polarimetric decomposition using PolInSAR coherence," in *Proc. IEEE Int. Geosci. Remote Sens. Symp.*, Vancouver, BC, Canada, Jul. 2011, pp. 1087–1090.

[41] Y. Yamaguchi, A. Sato, W. M. Boerner, R. Sato, and H. Yamada, "Four-component scattering power decomposition with rotation of coherency matrix," *IEEE Trans. Geosci. Remote Sens.*, vol. 49, no. 6, pp. 2251–2258, Jun. 2011.

[42] J. J. Van Zyl, M. Arii, and Y. Kim, "Model-based decomposition of polarimetric SAR covariance matrices constrained for nonnegative eigenvalues," *IEEE Trans. Geosci. Remote Sens.*, vol. 49, no. 9, pp. 3452–3459, Sep. 2011.

[43] I. Hajnsek, T. Jagdhuber, H. Schcon, and K. P. Papathanassiou, "Potential of estimating soil moisture under vegetation cover by means of PolSAR," *IEEE Trans. Geosci. Remote Sens.*, vol. 47, no. 2, pp. 442–454, Feb. 2009.

[44] O. Antropov, Y. Rauste, and T. Hame, "Volume scattering modeling in PolSAR decompositions: Study of ALOS PALSAR data over boreal forest," *IEEE Trans. Geosci. Remote Sens.*, vol. 49, no. 10, pp. 3838–3848, Oct. 2011.

[45] J. J. Sharma, I. Hajnsek, K. P. Papathanassiou, and A. Moreira, "Polarimetric decomposition over glacier ice using long-wavelength airborne PolSAR," *IEEE Trans. Geosci. Remote Sens.*, vol. 49, no. 1, pp. 519–535, Jan. 2011.

[46] M. Shimada, "Model-based polarimetric SAR calibration method using forest and surface-scattering targets," *IEEE Trans. Geosci. Remote Sens.*, vol. 49, no. 5, pp. 1712–1733, May 2011.

[47] J. S. Lee, D. L. Schuler, T. L. Ainsworth, E. Krogager, D. Kasilingam, and W. M. Boerner, "On the estimation of radar polarization orientation shifts induced by terrain slopes," *IEEE Trans. Geosci. Remote Sens.*, vol. 40, no. 1, pp. 30–41, Jan. 2002.

[48] K. Iribe and M. Sato, "Analysis of polarization orientation angle shifts by artificial structures," *IEEE Trans. Geosci. Remote Sens.*, vol. 45, no. 11, pp. 3417–3425, Nov. 2007.

[49] H. Kimura, "Radar polarization orientation shifts in built-up areas," *IEEE Geosci. Remote Sens. Lett.*, vol. 5, no. 2, pp. 217–221, Apr. 2008.

[50] F. Xu and Y. Q. Jin, "Deorientation theory of polarimetric scattering targets and application to terrain surface classification," *IEEE Trans. Geosci. Remote Sens.*, vol. 43, no. 10, pp. 2351–2364, Oct. 2005.

[51] J. S. Lee and T. L. Ainsworth, "The effect of orientation angle compensation on coherency matrix and polarimetric target decompositions," *IEEE Trans. Geosci. Remote Sens.*, vol. 49, no. 1, pp. 53–64, Jan. 2011.

[52] S. W. Chen, M. Ohki, M. Shimada, and M. Sato, "Deorientation effect investigation for model-based decomposition over oriented built-up areas," *IEEE Geosci. Remote Sens. Lett.*, vol. 10, no. 2, pp. 273–277, Mar. 2013.

[53] [Online]. Available: http://en.wikipedia.org/wiki/Ishinomaki,_Miyagi

[54] [Online]. Available: http://www.tsunami.civil.tohoku.ac.jp/tohoku2011/map/miyagi/

[55] [Online]. Available: http://www.data.jma.go.jp/obd/stats/etrn/index.php

[56] S. R. Cloude and K. P. Papathanassiou, "Polarimetric SAR interferometry," *IEEE Trans. Geosci. Remote Sens.*, vol. 36, no. 5, pp. 1551–1565, Sep. 1998.

[57] T. Tadono, M. Shimada, H. Murakami, and J. Takaku, "Calibration of PRISM and AVNIR-2 onboard ALOS "Daichi"," *IEEE Trans. Geosci. Remote Sens.*, vol. 47, no. 12, pp. 4042–4050, Dec. 2009.

[58] J. S. Lee, J. H. Wen, T. L. Ainsworth, K. S. Chen, and A. J. Chen, "Improved sigma filter for speckle filtering of SAR imagery," *IEEE Trans. Geosci. Remote Sens.*, vol. 47, no. 1, pp. 202–213, Jan. 2009.

[59] S. W. Chen, X. S. Wang, and M. Sato, "PolInSAR complex coherence estimation based on covariance matrix similarity test," *IEEE Trans. Geosci. Remote Sens.*, vol. 50, no. 11, pp. 4699–4710, Nov. 2012.

[60] G. Margarit, J. J. Mallorqui, and L. Pipia, "Polarimetric characterization and temporal stability analysis of urban target scattering," *IEEE Trans. Geosci. Remote Sens.*, vol. 48, no. 4, pp. 2038–2048, Apr. 2010.

[61] A. Ferretti, C. Prati, and F. Rocca, "Permanent scatterers in SAR interferometry," *IEEE Trans. Geosci. Remote Sens.*, vol. 39, no. 1, pp. 8–20, Jan. 2001.

[62] S. W. Chen and M. Sato, "General polarimetric model-based decomposition for coherency matrix," in *Proc. IEEE Int. Geosci. Remote Sens. Symp.*, Munich, Germany, Jul. 2012.

Si-Wei Chen (S'10) received the B.E. degree in information engineering from National University of Defense Technology, Changsha, China, in 2007 and the Ph.D. degree in environmental studies from Tohoku University, Sendai, Japan, in 2012.

He was a Research Assistant with the Remote Sensing Group, the Center for Northeast Asian Studies, Tohoku University from 2011 to 2012. He has published 7 journal papers and more than 10 conference proceedings. His research interests include radar polarimetry, polarimetric synthetic aperture radar (SAR), polarimetric SAR interferometry, and natural disaster study.

Dr. Chen is a recipient of the Outstanding Postgraduate Innovation Grant from National University of Defense Technology (2008–2009), and the Young Researcher Award from IEEE GRSS-Japan chapter in 2011. He received the Tohoku University President Fellowship in 2011. He is a reviewer for IEEE TRANSACTIONS ON GEOSCIENCE and REMOTE SENSING and IEEE GEOSCIENCE AND REMOTE SENSING LETTERS. He is a co-investigator of European Space Agency Earth Observation Campaign.

Motoyuki Sato (S'79–M'80–SM'02–F'10) received the B.E., M.E., and Dr.Eng. degrees in information engineering from the Tohoku University, Sendai, Japan, in 1980, 1982, and 1985, respectively.

Since 1997, he has been a Professor at Tohoku University, Sendai, and a Distinguished Professor of Tohoku University, since 2007, and he has been the Director of the Center for Northeast Asian Studies, Tohoku University, since 2009. From 1988 to 1989, he was a Visiting Researcher at the Federal German Institute for Geoscience and Natural Resources (BGR), in Hannover, Germany. His current interests include transient electromagnetics and antennas, radar polarimetry, ground penetrating radar (GPR), borehole radar, electromagnetic induction sensing, interferometric and polarimetric synthetic aperture radar. He has conducted the development of GPR sensors for humanitarian demining, and his sensor ALIS which is a hand-held dual sensor, has detected more than 80 mines in mine fields in Cambodia since May 2009. He is a Visiting Professor at Jilin University, China, Delft University of Technology, The Netherlands, and Mongolian University of Science and Technology.

Dr. Sato is a member of the GRSS AdCom (2006-) where he is responsible for specialty symposia and Asian issues. He is an Associate Editor of the IEEE GRSS NEWSLETTER, and a Guest Editor of the special issue of GPR2006 and GPR2010 in the IEEE TRANSACTIONS ON GEOSCIENCE AND REMOTE SENSING. He was the Chair of the IEEE GRSS Japan Chapter (2006 to 2007). He served as the General Chair of IGARSS2011.